Acta of Bioengineering and Biomechanics
Vol. 19, No. 3, 2017

Original paper
DOI: 10.5277//ABB-00775-2016-05

Investigation of blood flow rheology using second-grade viscoelastic model (Phan-Thien–Tanner) within carotid artery

ABAS RAMIAR, MORSAL MOMENI LARIMI*, ALI AKBAR RANJBAR

Faculty of Mechanical Engineering, Noshirvani University of Technology, Babol, Iran.

Purpose: Hemodynamic factors, such as Wall Shear Stress (WSS), play a substantial role in arterial diseases. In the larger arteries, such as the carotid artery, interaction between the vessel wall and blood flow affects the distribution of hemodynamic factors. The fluid is considered to be non-Newtonian, whose flow is governed by the equation of a second-grade viscoelastic fluid and the effects of viscoelastic on blood flow in carotid artery is investigated. *Methods*: Pulsatile flow studies were carried out in a 3D model of carotid artery. The governing equations were solved using finite volume C++ based on open source code, OpenFOAM. To describe blood flow, conservation of mass and momentum, a constitutive relation of simplified Phan-Thien–Tanner (sPTT), and appropriate relations were used to explain shear thinning behavior. *Results*: The first recirculation was observed at $t = 0.2$ s, in deceleration phase. In the acceleration phase from $t = 0.3$ s to $t = 0.5$ s, vortex and recirculation sizes in bulb regions in both ECA and ICA gradually increased. As is observed in the line graphs based on extracted data from ICA, at $t = 0.2$ s, τ_{yy} is the maximum amount of wall shear stress and τ_{xy} the minimum one. The maximum shear stress occurred in the inner side of the main branch (inner side of ICA and ECA) because the velocity of blood flow in the inner side of the bulb region was maximum due to the created recirculation zone in the opposite side in this area. *Conclusions*: The rheology of blood flow and shear stress in various important parts (the area that are in higher rates of WSS such as bifurcation region and the regions after bulb areas in both branches, Line1–4 in Fig. 7) were also analyzed. The investigation of velocity stream line, velocity profile and shear stress in various sections of carotid artery showed that the maximum shear stress occurred in acceleration phase and in the bifurcation region between ECA and ICA which is due to velocity gradients and changes in thinning behavior of blood and increasing strain rate in Newtonian stress part.

Key words: *carotid artery, viscoelastic model, pulsatile flow, shear stress, OpenFOAM*

1. Introduction

Blood flow (or hemodynamics) problems have received considerable attention due to their importance in physio-pathology. Blood circulation has various functions in human body, e.g. transporting nutrients and oxygen, removing metabolic products and carbon dioxide, etc. Several authors investigated blood flow problems in various geometrical aspects with different biological fluids [8], [17], [26]–[28]. Sinha and Misra [24] investigated blood flow under externally applied magnetic field. Sud et al. [25] analyzed the effect of a moving magnetic field on blood. Reddy et al. [23] contributed to a mathematical model on couple stress fluid flow through stenosis annular region and found that impedance would increase with rises in height and length of stenosis. Hayat et al. [9] studied the effects of Hall on peristaltic motion of couple stress fluid in an inclined asymmetric channel with heat and mass transfer. Adesanya and Makinde [1] investigated the influence of couple stress fluid flow on steady thin flow down heated inclined plate and found that the effect of couple stress parameter would be to cut down flow velocity and temperature distribution. Prakash et al. [21] reported that the size of stenosis would decrease volumetric flow rate and increase wall shear stress as well as impedance. Makinde [16] obtained

* Corresponding author: Morsal Momeni Larimi, Faculty of Mechanical Engineering, Noshirvani University of Technology, Juybar-Mazandaran-Iran, 4777119871 Juybar, Iran. Phone: +9801142552573, e-mail: morsalmomeni@yahoo.com

Received: October 31st, 2016
Accepted for publication: January 24th, 2017

asymptotic approximations of oscillatory flow through a tube of varying cross sections with permeable isothermal wall and analyzed that fluid absorption at the wall would decrease the magnitude of wall shear stress, pressure drop and wall heat transfer rate, but the influence of oscillation of the fluid could still be significant at a high rate of fluid absorption at the wall. Prakash and Makinde [22] observed that impedance would reduce due to magnetic field effect when patients experienced thermal radiation therapy. Non-Newtonian models have been employed with increasing frequency in flow simulations of various vascular components, such as aorta [11], [15], [19], cerebral [2], [4] and coronary arteries [14], [18]. In all these studies, generalized Newtonian expressions were adopted to better capture the complex behavior of the fluid under steady state conditions. In [12], the effect of non-uniform magnetic field on wall shear stress and streamline in a 2D bifurcation considering blood as a Newtonian fluid was studied. The results showed a significant effect on wall shear and stream line in magnetic affected areas. Also in [13], the magnetic nano-particles and blood flow behavior in carotid artery in drug delivery application were investigated. In this study, the blood flow is considered pulsatile and the changes in blood and nano-particles behavior in various time in ECA and ICA have been studied.

The aim of the present study was to analyze peristaltic blood flow in carotid artery considering the influence of viscoelasticity on rheological characteristics of human blood in the hope to provide a good understanding of blood flow in carotidal blood vessels. The resulting differential equation was solved numerically using C++ based on finite volume software, OpenFOAM. The impact of all physical parameters was plotted and discussed. Blood flow was considered non-Newtonian, pulsatile, and incompressible. A simplified Phan-Thien–Tanner (sPTT) viscoelastic model was applied to investigate blood behavior.

Governing equations

This section deals with to viscoelastic incompressible laminar flow in carotid artery with rigid wall. As blood is assumed to behave as an incompressible fluid and in a large vessel, it can be considered an isotropic continuum medium. Mass and momentum equations used were

$$\nabla . u = 0 , \tag{1}$$

$$\rho\left(\frac{\partial U}{\partial y} + U.\nabla(Uu)\right) = -\nabla p + \nabla.\tau , \tag{2}$$

where U is the velocity vector, and τ and p are the stress and pressure, respectively. The simplified Phan-Thien–Tanner (sPTT) model was used as constitutive equation, in which total stress was separated into Newtonian and polymeric stress in the form of Eq. (3), where τ_s is the stress caused by Newtonian solvent and τ_p is the polymeric stress contribution to the total stress.

$$\tau = \tau_s + \tau_p . \tag{3}$$

In Newtonian solution, the relationship between stress and strain rate is in the form of Eq. (4). In this equation, η_s is the viscosity related to Newtonian solution and $\dot{\gamma}$ is the shear rate tensor. The shear rate tensor could be presented as Eq. (5).

$$\tau_s = \eta_s \dot{\gamma} , \tag{4}$$

$$\dot{\gamma} = \nabla u + (\nabla u)^T . \tag{5}$$

Extra elastic contribution corresponding to polymeric part τ_P was obtained by solving an appropriate constitutive differential equation. In sPTT, in which α = 0, polymeric stress can be obtained from the equation

$$\left(1 + \frac{\varepsilon_{p_k}\lambda_{p_k}}{\eta_{p_k}}\mathrm{tr}(\tau_{p_k})\right)\tau_{p_k} + \lambda_{p_k}\tau_{p_k} + \alpha_{p_k}\frac{\lambda_{p_k}}{\eta_{p_k}}\{\tau_{in_k}.\tau_{nj_k}\} = \eta_p\dot{\gamma}. \tag{6}$$

In this model, τ_p includes four modes (N = 4); three coefficients in each mode, i.e., relaxation time (λ_{pk}), viscosity contribution to zero shear viscosity (η_{pk}), and extensibility coefficient (ε) or the mobility factor (α).

2. Geometry and boundary conditions

The geometry studied in this research was carotid artery, consisting of two main branches, i.e., internal carotid artery (ICA), and external carotid artery (ECA) as well as one inlet called common carotid artery (CCA). Two branches were added to this geometry at ICA and ECA. All sizes of the geometry considered are shown in Fig. 1.

The fully developed pulsatile flow at the inlet regarded as a profile is shown by equation (7).

$$U_r = U_{\max}\left(1 - \frac{r^2}{R^2}\right), \quad U_{\max} = \frac{3}{2}U_{in}, \tag{7}$$

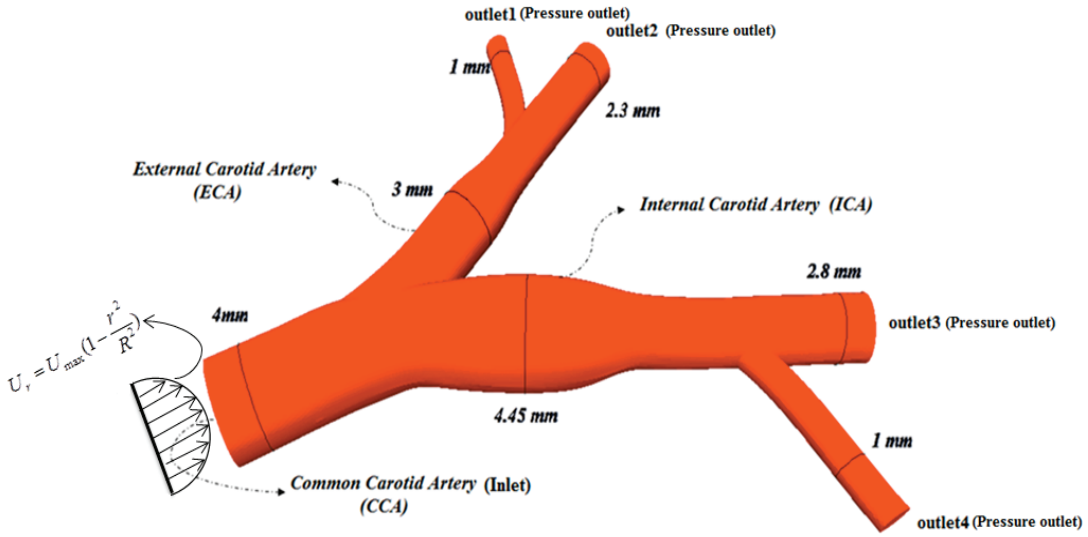

Fig. 1. Geometry of carotid artery investigated in this study

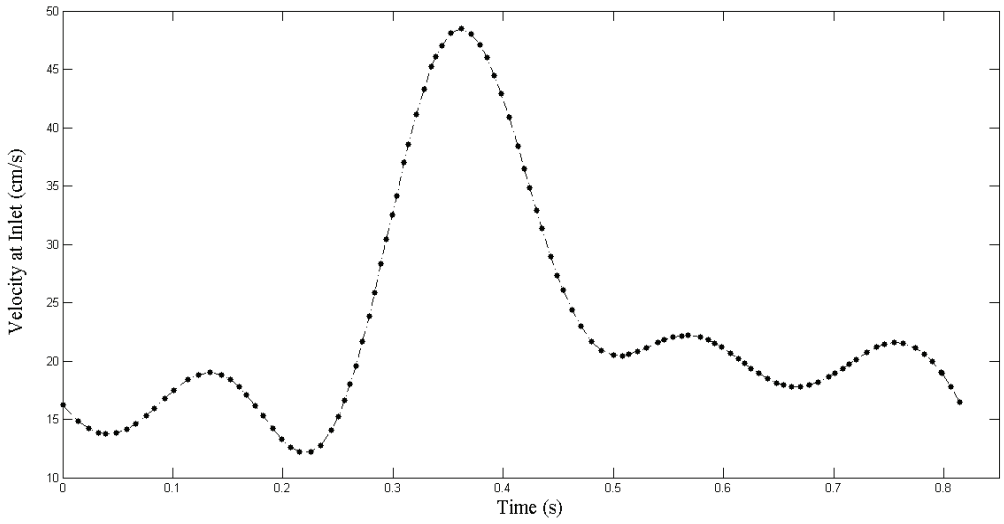

Fig. 2. Velocity at the inlet (CCA) [20]

where U_{in} is considered as a pulsatile flow which is shown in Fig. 2. Since blood density was considered 1050 kg/m^3, the magnitude of average Reynolds number at the inlet was in a laminar regime. At the outlets (outlet1–outlet4), the pressure outlet boundary condition has been used.

Fluid flow was selected non-Newtonian and simulated using viscoelastic sPTT model as mentioned in the previous section. All physical parameters and coefficients applied in this simulation are presented in Table 1.

In this simulation, PISO algorithm was used for velocity-pressure coupling. Second order upwind scheme was used for the discretization of both convective and Laplacian terms in momentum Gauss linear schemes applied. Three dimensional and incompressible Navier–Stokes equations were solved by finite-volume open source software OpenFOAM. Velocity convergence criteria were less than 10^{-6}; also less than 10^{-6} for the whole four modes in shear stress equation. All data were extracted after the fourth pulse when the results were permanent and stable simultaneously in various pulses.

Table 1. Simulation parameters quantities [7]

ρ (kg/m^3)	Fluid density		1050
Simplified Phan-Thien–Tanner(sPTT)-(α = 0)			
Mode (i)	$\eta_{pi}(pa.s)$	$\lambda_i(s)$	ε_i
1	0.05	7	0.2
2	0.001	0.4	0.5
3	0.001	0.04	0.5
4	0.0016	0.006	0.5

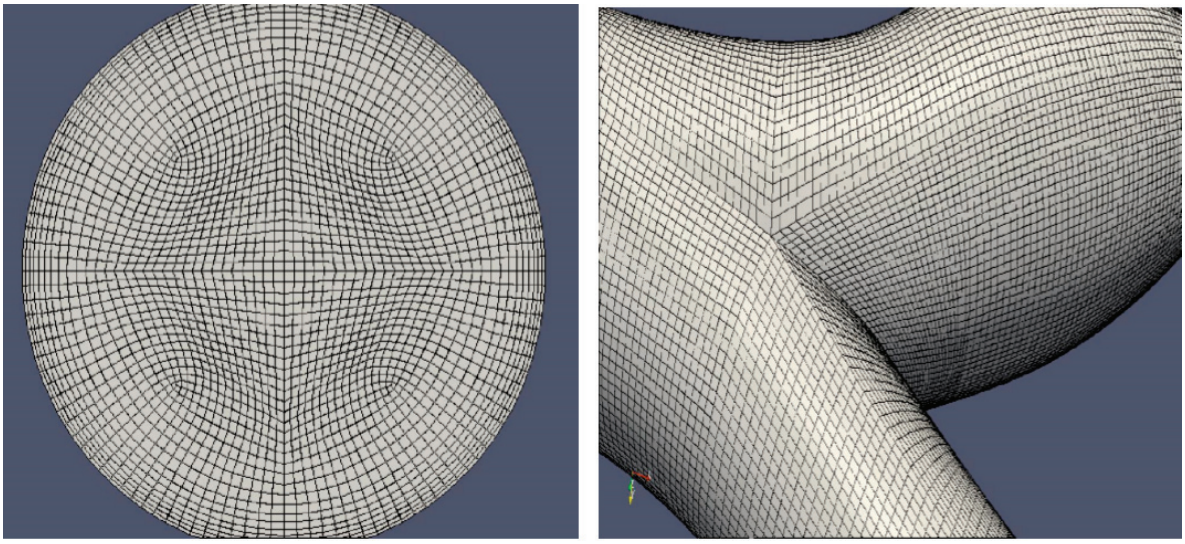

Fig. 3a. Gird generated in two sections

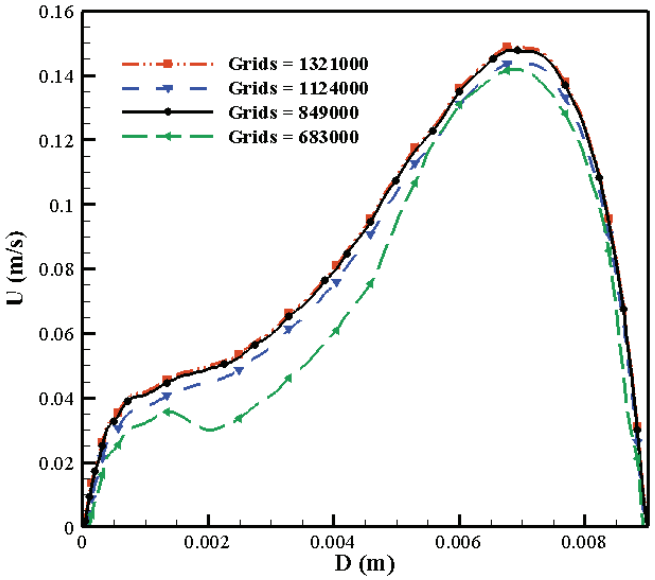

Fig. 3b. Mesh independence for four grids number

Fig. 3. Mesh independence and grid generated on geometry

The flow domains were meshed with hexahedral cells using Gambit software and the mesh generated in two sections are shown in Fig. 3a. For mesh independence, the velocity profile in the cross section of bulb region in ICA (specified in Fig. 1) at the acceleration phase and t = 0.4 s has been investigated. The results indicate the maximum differences in velocity magnitude between the two maximum grids are less than 3%. Therefore, the grid with 1 124 000 elements is used for the simulations, considering the compromise of computational time and accuracy.

3. Results

3.1. Investigating blood flow streamlines in carotid artery

As one of the most important areas in carotid artery is known to be the bulb region in ICA, to better understand blood behavior in this region, velocity contour and streamlines of a cross section in the middle of the region were investigated, Fig. 4. Velocity

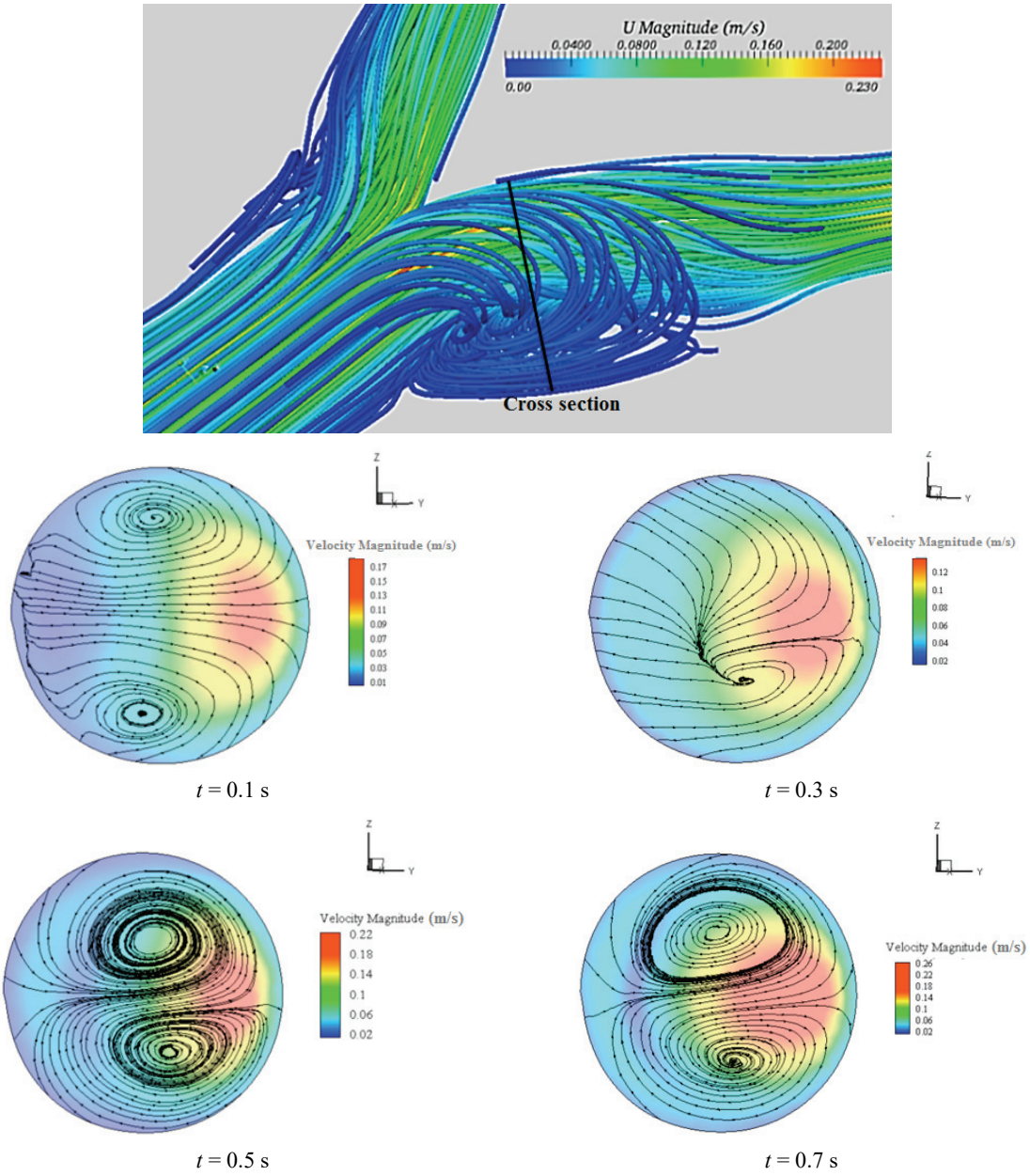

Fig. 4. Streamlines in a cross section in the middle of the bulb region in ICA

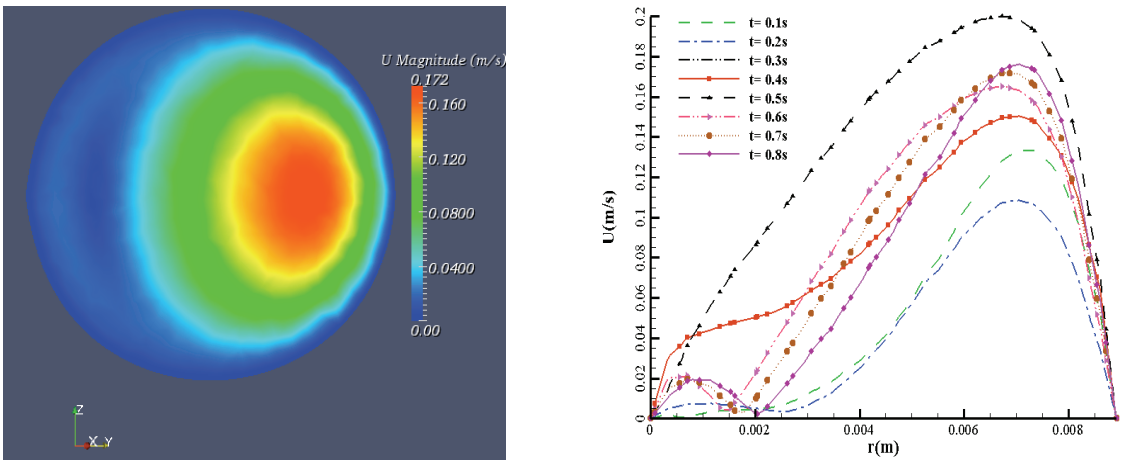

Fig. 5. Velocity profile in ICA bulb region cross section at various times

changes of blood flow behavior and vortex sizes at various times are shown in this figure.

Velocity profiles at various times in a cross section in ICA bulb region are shown in Fig. 5. As t = 0.6 s, at the beginning of the profile, the effect of recirculation as well as the changes in velocity and mass flux in the cross section can be illustrated through the profile.

3.2. Investigating the wall shear stress

Changes in the wall shear stress in carotid artery at various times were investigated (Fig. 6). These changes could be considered really important and noticeable, especially in treating some diseases such as aneurysm. This disease tends to appear most of

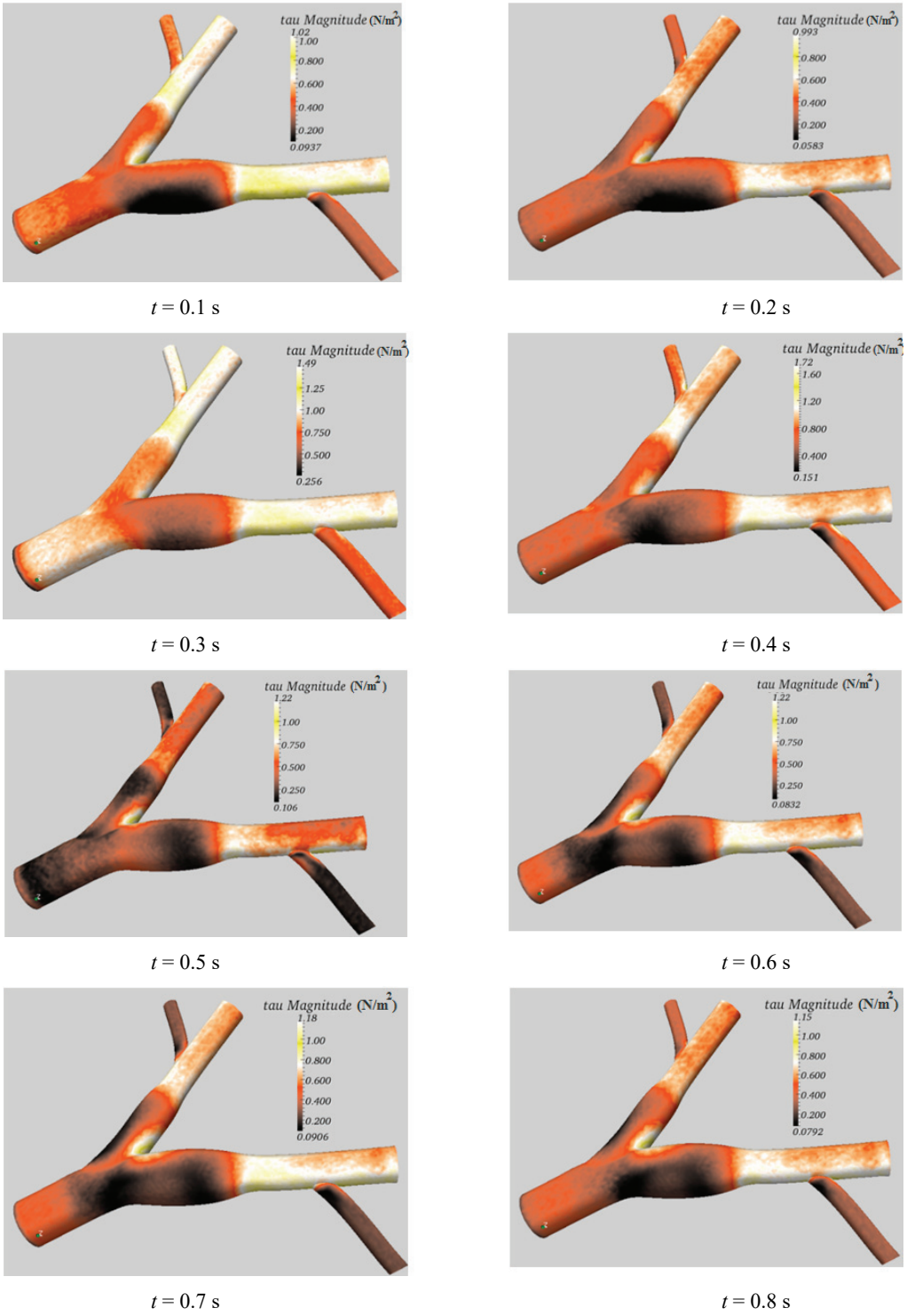

t = 0.1 s t = 0.2 s

t = 0.3 s t = 0.4 s

t = 0.5 s t = 0.6 s

t = 0.7 s t = 0.8 s

Fig. 6. Changes in the wall shear stress at various times

the time by rising the wall shear to the critical amount.

3.3. Investigating changes in the wall shear stress in important area

To better understand the wall shear behavior at various times in pulsatile flow in carotid artery, four main lines from most important areas of this artery were selected and the changes in the wall shear stress in these areas were investigated (Fig. 7). In the first place, bulb regions in both ECA and ICA were investigated. Subsequently, the wall shear stress in Line 3 and Line 4 was investigated.

3.4. Investigating the shear-thinning effect on blood shear stress in ICA and ECA

The characteristics of blood flow in carotid are shown in Fig. 8 using the wall shear stress of the whole modes at various times in a cross section of the bulb region in ICA.

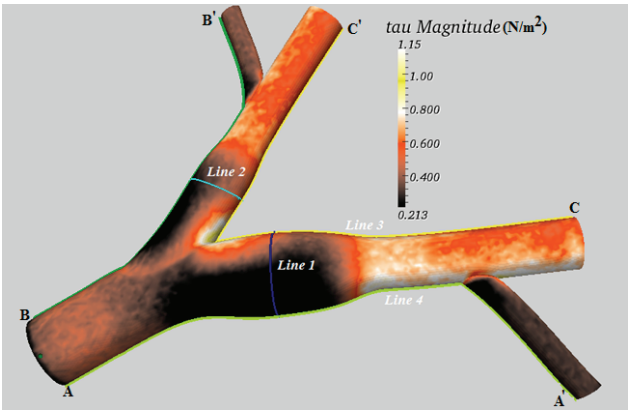

(a) Various parts considered to investigate shear stress

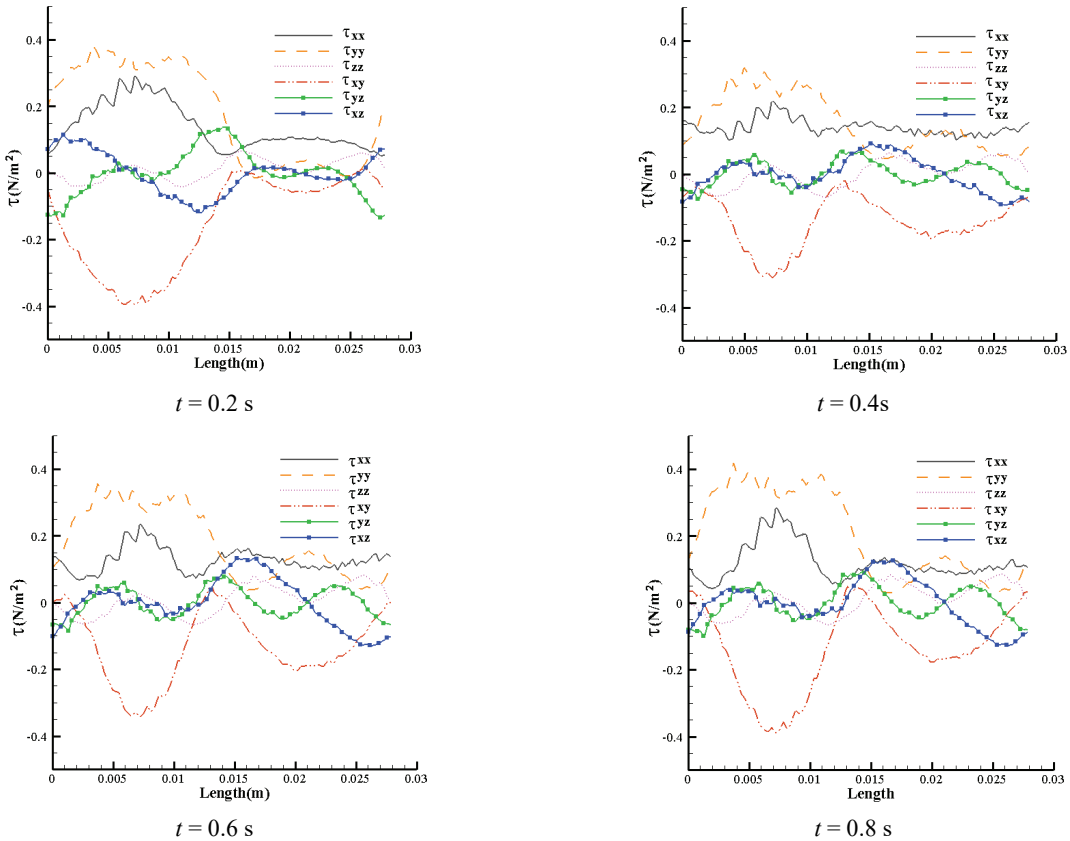

$t = 0.2$ s

$t = 0.4$s

$t = 0.6$ s

$t = 0.8$ s

(b) Data extracted from Line 1

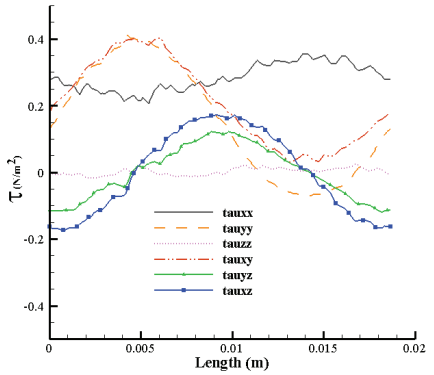

$t = 0.2$ s

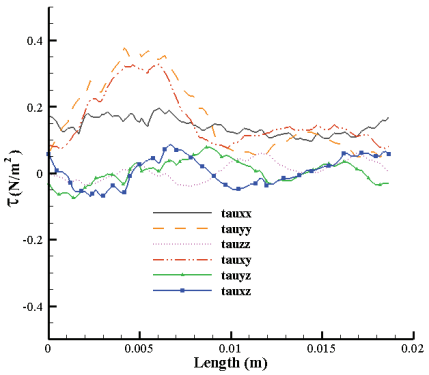

$t = 0.4$ s

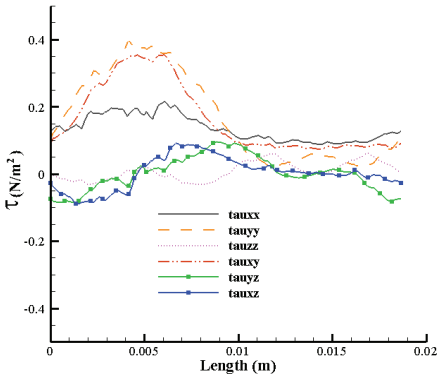

$t = 0.6$ s

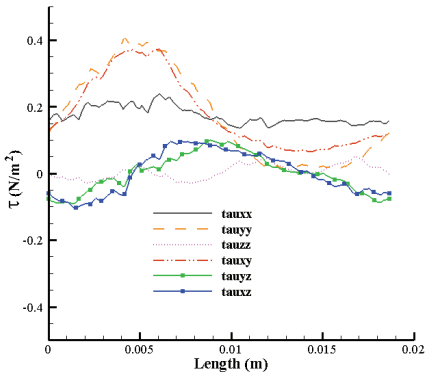

$t = 0.8$ s

(c) Data extracted from Line 2

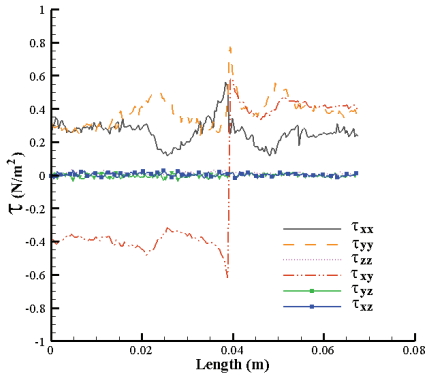

$t = 0.2$ s

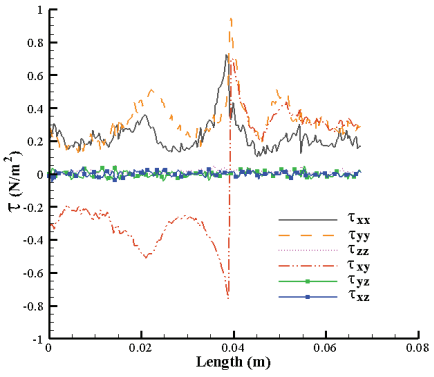

$t = 0.4$ s

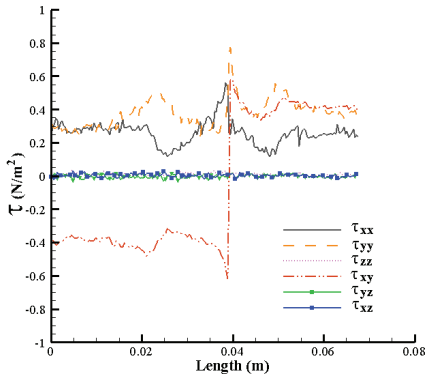

$t = 0.6$ s

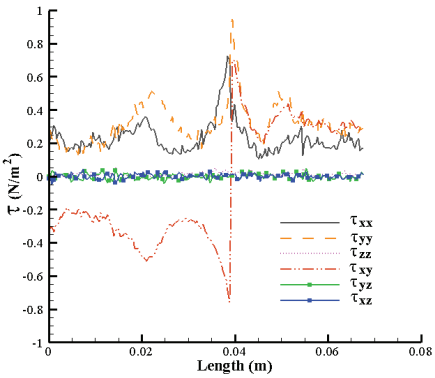

$t = 0.8$ s

(d) Data extracted from Line 3 (C-C′)

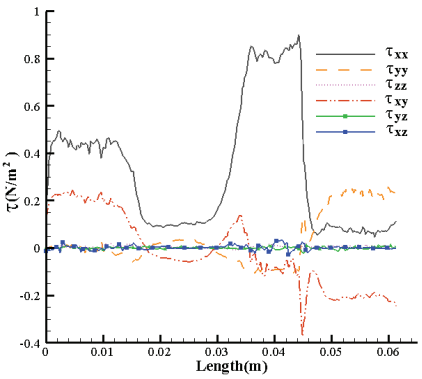

t = 0.2 s

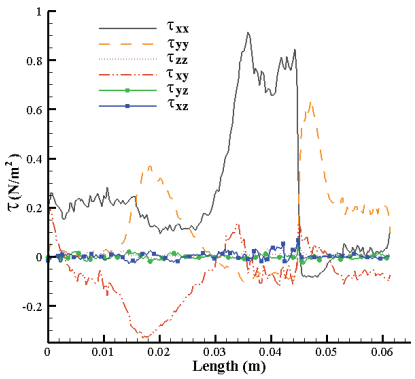

t = 0.4 s

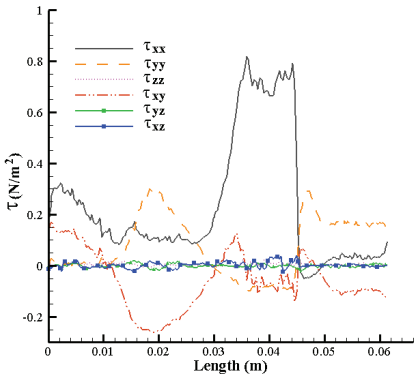

t = 0.6 s

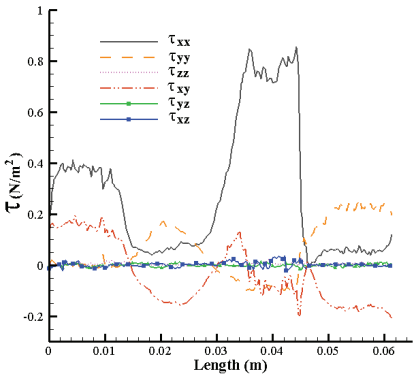

t = 0.8 s

(e) Data extracted from Line 4 (A-A′)

Fig. 7. The wall shear stress in various sections

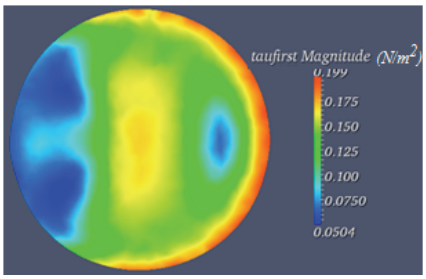

t = 0.4 s

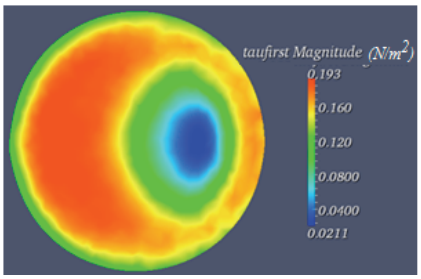

t = 0.6 s

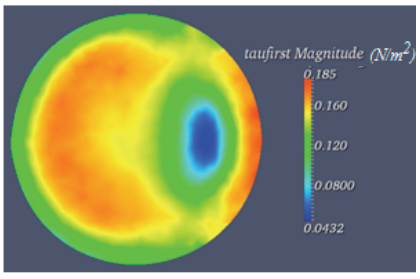

t = 0.8 s

(a) First mode

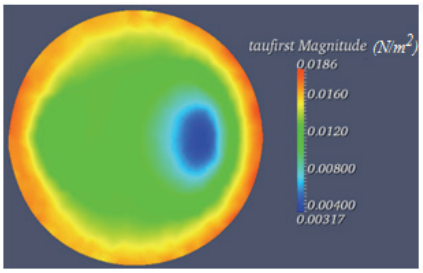

t = 0.4 s

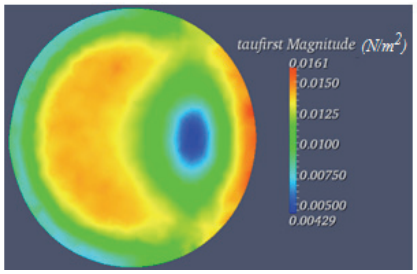

t = 0.6 s

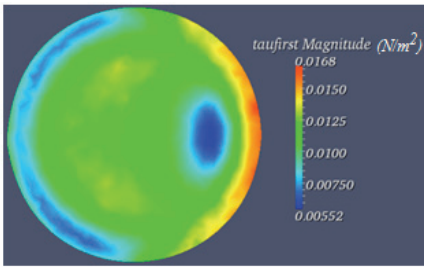

t = 0.8 s

(b) Second mode

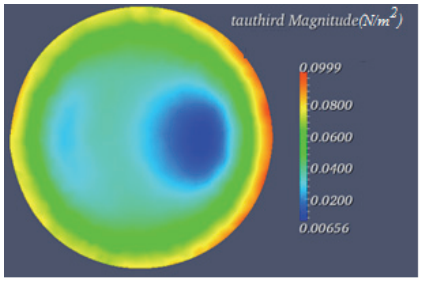

$t = 0.4$ s

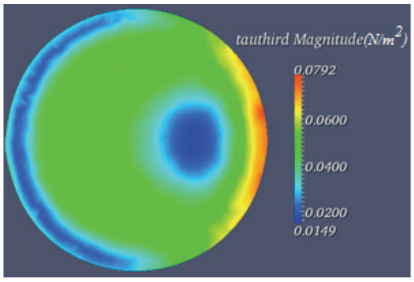

$t = 0.6$ s

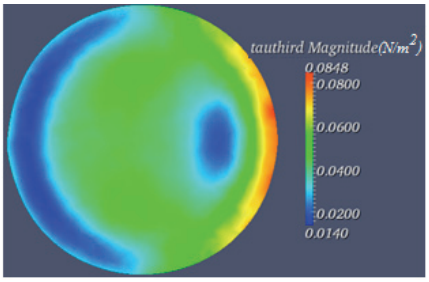

$t = 0.8$ s

(c) Third mode

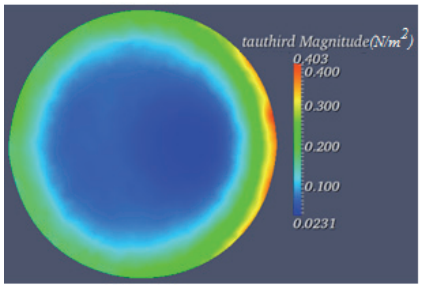

$t = 0.4$ s

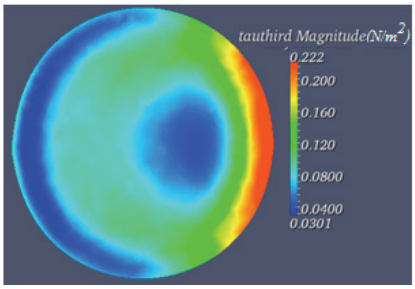

$t = 0.6$ s

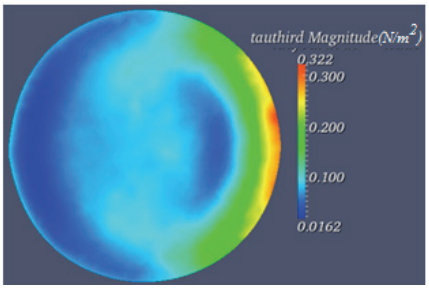

$t = 0.8$ s

(d) Fourth mode

Fig. 8. Shear stress contour in ICA bulb cross section in all four modes

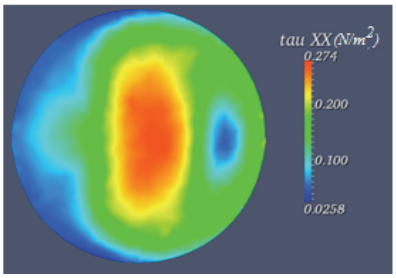

$t = 0.2$ s

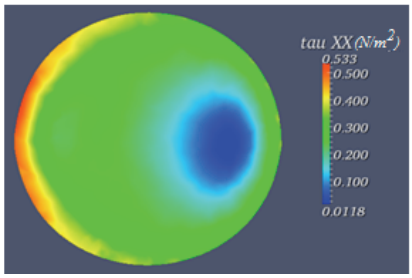

$t = 0.04$ s

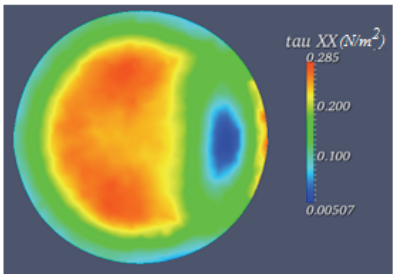

$t = 0.8$ s

τ_{xx}

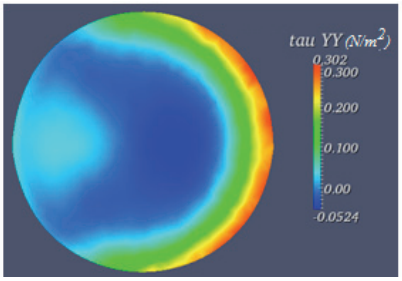

$t = 0.2$ s

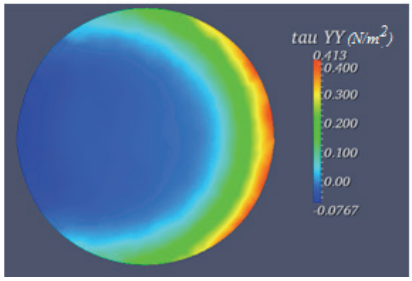

$t = 0.04$ s

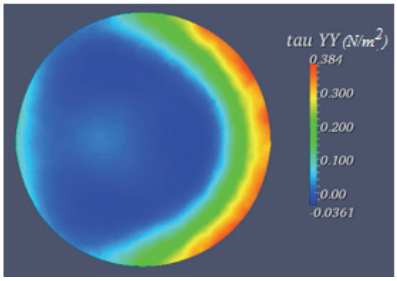

$t = 0.8$ s

τ_{yy}

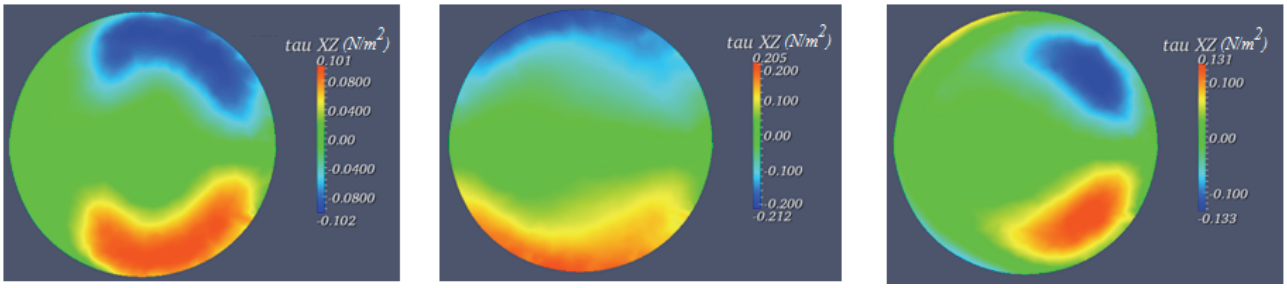

$t = 0.2$ s $t = 0.04$ s $t = 0.8$ s

τ_{xz}

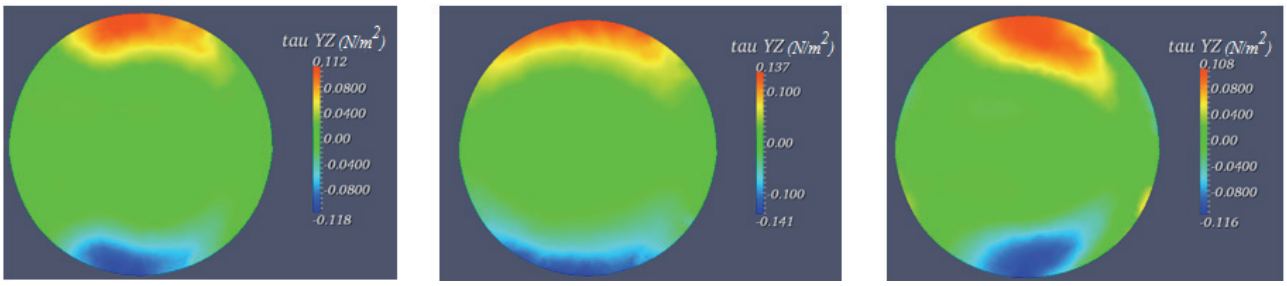

$t = 0.2$ s $t = 0.04$ s $t = 0.8$ s

τ_{yz}

Fig. 9. Blood flow stress contour in a vertical section of bulb region in ICA

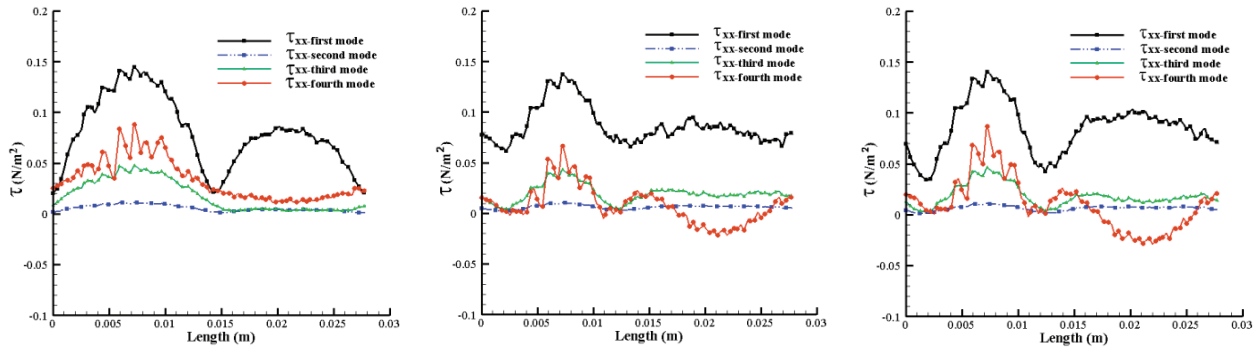

$t = 0.2$ s $t = 0.6$ s $t = 0.6$ s

τ_{xx}

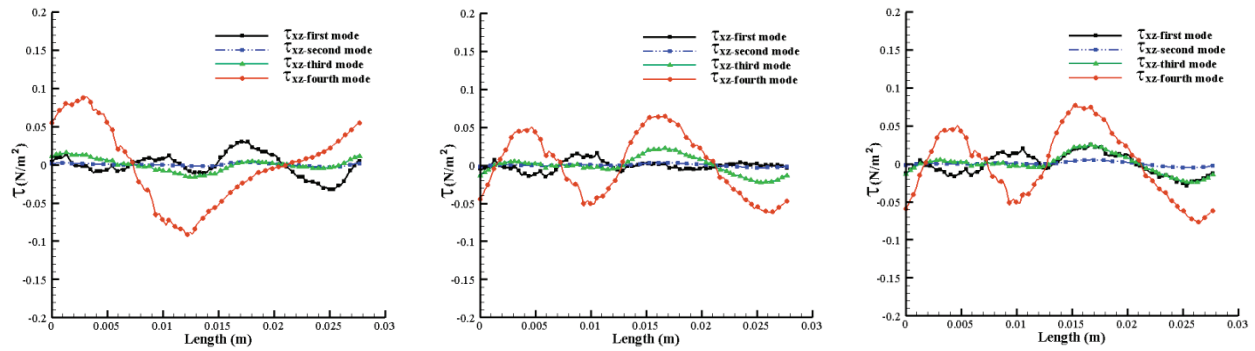

$t = 0.2$ s $t = 0.6$ s $t = 0.8$ s

τ_{xz}

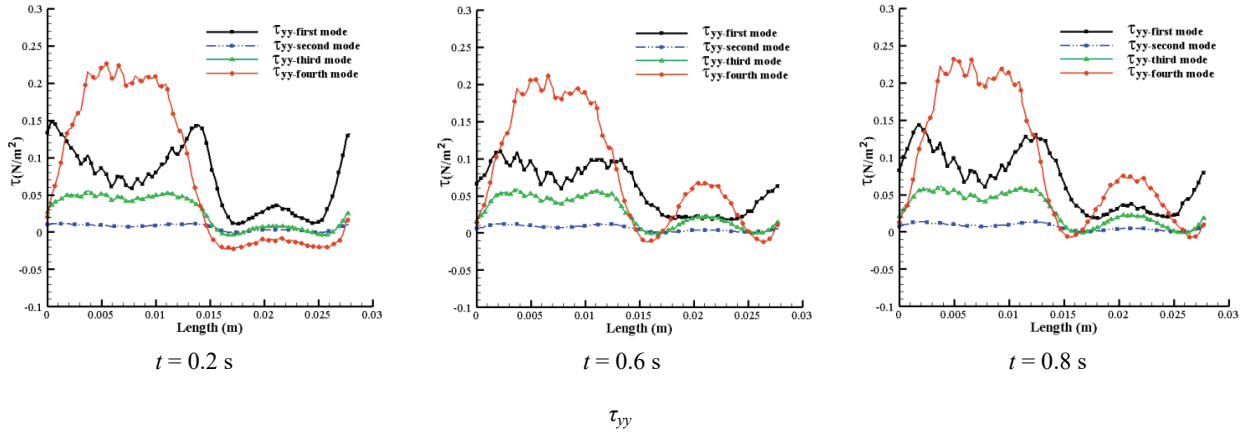

t = 0.2 s t = 0.6 s t = 0.8 s

τ_{yy}

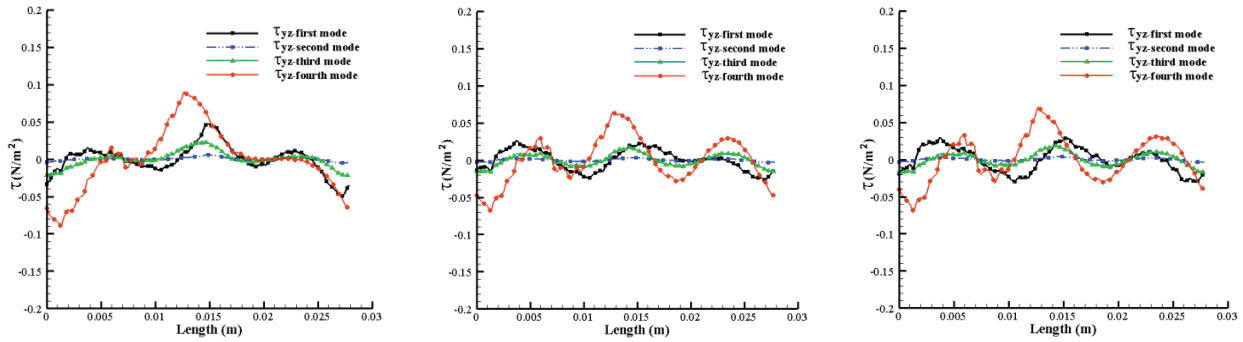

t = 0.2 s t = 0.6 s t = 0.8 s

τ_{yz}

Fig. 10. Wall shear stress changes in whole modes in a cross section of ICA

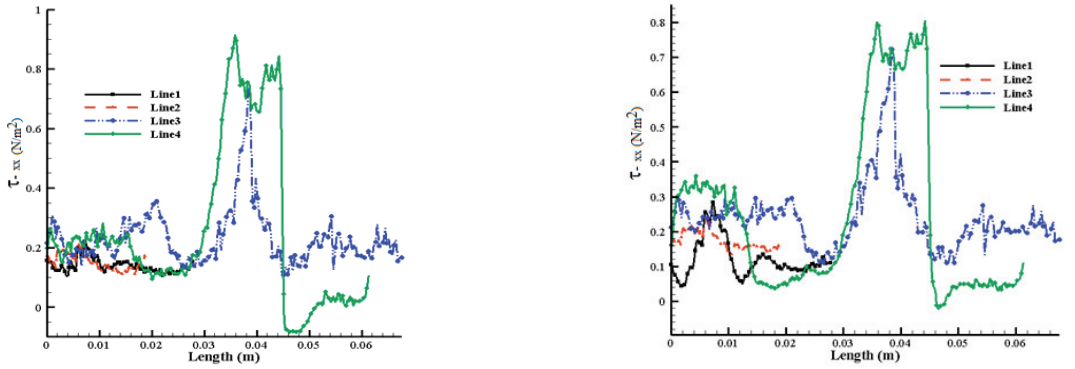

t = 0.2 s t = 0.8 s

τ_{xx}

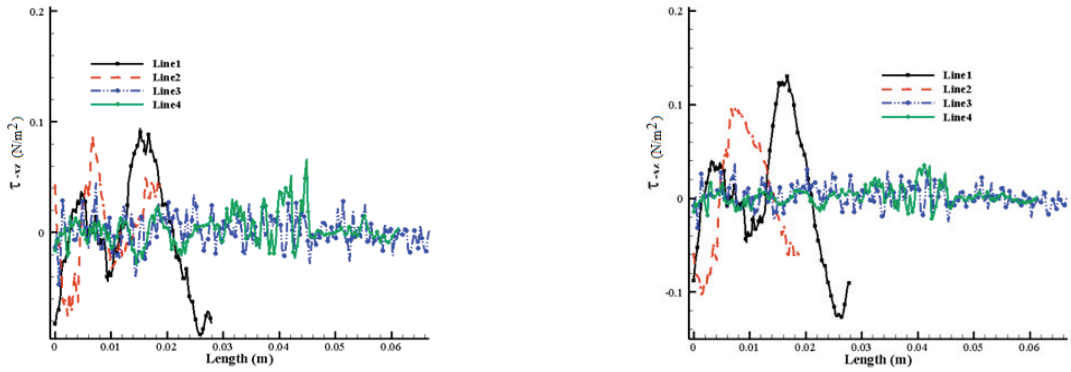

t = 0.2 s t = 0.8 s

τ_{xz}

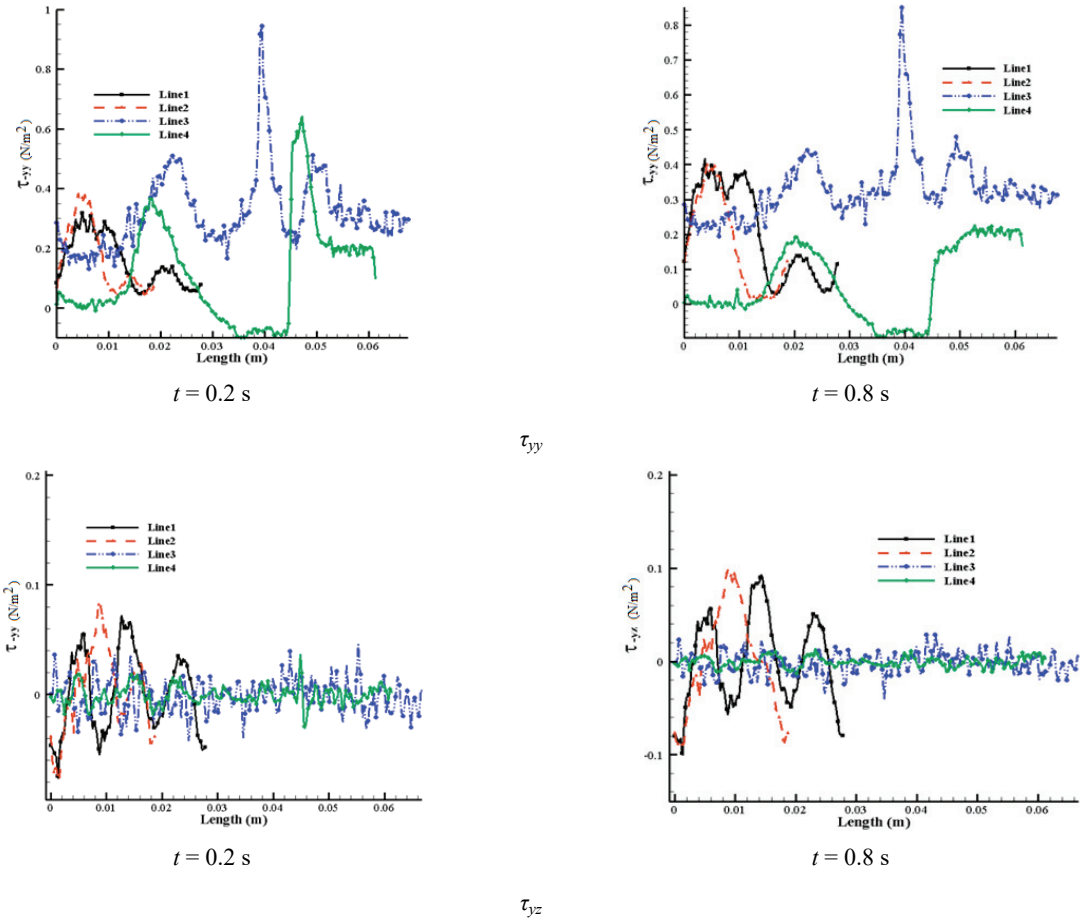

Fig. 11. Comparison of the wall shear stress in various sections of carotid artery

Figure 9 illustrates the internal stress of blood flow of ICA bulb cross-section at three specified times. As can be seen in Fig. 10, the behavior of τ_{xx} is completely the same as $\tau_{\text{magnitude}}$, and τ_{yy} has more influence on the shear stress near the wall. Therefore, it can be said that in this area τ_{xx} and τ_{yy} have more effects on predicting shear stress behavior of blood.

In addition, τ_{xz} and τ_{yz} are symmetric in horizontal line due to the rotation of fluid in this area. Since the shear rate in arteries on the wall is considered important, the changes in the wall shear stress in Line 1 in ICA (Fig. 7) were investigated.

The results showed that in the τ_{xx} of the first mode and in other shear stresses of the fourth mode higher measures of shear stress were predicted. At all times, the wall shear stress increased because the pulsating blood and oscillation of strain rate fluctuated.

Finding critical and high risk regions for various diseases such as rapture risk and aneurysm or atherosclerosis can be an important goal in this study. Regions with lower shear stress are comfortable areas for atherosclerosis, and by contrast, regions with high shear rate can be in rapture dangerous or aneurysm diseases. Therefore, a comparison between the wall shear stress in the four lines considered was done (Fig. 11). As one can see from Fig. 11, in Line 3 in bifurcation region and in Line4 after bulb area, WSS experienced its maximum rate in comparison with other regions and this result shows that these two regions can be considered as high risk areas in this artery.

4. Discussion

In this study, the behavior of blood flow in carotid artery and the wall shear changes were investigated, with blood being considered as a viscoelastic fluid. For this purpose, the second-grade viscoelastic model (Phan-Thien–Tanner) and an open source code (OpenFOAM) were applied for simulations. To analyse the behavior of blood, especially in ICA and ECA (Fig. 4), streamlines and velocity profile as well as changes in the wall shear stresses in various regions were investigated, and critical area for atherosclerosis disease and also high risk region for probable rapture or aneurysm were identified. The behavior of recircu-

lation, as predicted, indicated that the size of recirculation in bulb regions in both ICA and ECA increased in the acceleration phase and then got smaller in size during deceleration phase, and consequently, changes in the size of the secondary flow experienced a similar behavior in both phases (Fig. 4 and Fig. 5). Botnar et al. [3] and Jozwik and Obidowski [10] in their studies also found similar behavior in ECA and ICA in velocity profile and recirculation and secondary flow in carotid artery. This behavior was also observed in our previous research, in which the blood was solved for both Newtonian and Carreau models [23]. A more detailed look at Fig. 6 shows that maximum shear stress occurs in the middle of two branches (between ECA and ICA), and the regions after the bulb area in both ECA and ICA due to increases in velocity gradient and velocity magnitude in these regions. It can also be seen that minimum shear stress is in the recirculation zone due to the fact that in this area the collision between blood flow and vessel wall reduces. The study of the wall shear stress in various specified lines (Fig. 7) suggested that for the line graphs based on data extracted from ICA, at $t = 0.2$ s, τ_{yy} is the maximum amount of the wall shear stress and τ_{xy} the minimum one. The maximum shear stress occurred on the inner side of the main branch (inner side of ICA and ECA) because the velocity of blood flow on the inner side of the bulb region was maximum due to the recirculation zone created on the opposite side of this area, whereas the minimum was seen on the outer side of the bulb region. A similar behavior of all shear stress was also seen in the smaller bulb region in ECA (Line 2). Comparing the line graphs of both bulb regions, it can be observed that the most noticeable difference between them is at τ_{xy} and τ_{xx}, τ_{yy}, τ_{xy} showing more effects on the magnitude of shear stress in these regions. The graph related to Line3 shows that the behaviors of all shear stress tend to be symmetric to the bifurcation area, in which all shear stress, especially τ_{xy}, soared. This could be due to the maximum velocity gradient and its effect on the shear thinning property of blood flow in this area. In the next line (Line4), changes in the wall shear stress from inlet to outlet 4 were considered. The result represented by a graph reveals that the wall shear stress along the line at various times tends to fluctuate. In addition, the maximum wall shear in this line (Line 4) can be seen in the area just after the bulb region which can be due to increases in velocity gradient in this region. In the area between the bulb region and sub-branch, τ_{xx}, plateaued, but after that sub-branches in ECA ($L = 0.048$) slashed. A look at the previous experimental results from other articles such as Wilde et al. [29] and Cibisa et al. [6] confirm similar regions for the maximum wall shear stress (bifurcation area and after bulb region). Similar to the previously considered lines, the influences of τ_{xx}, τ_{yy}, τ_{xy} are more noticeable than the other shear stress. A more detailed look at the contours in this figure shows that in all four modes and at all times, maximum wall shear stress is in the area with high velocity due to the fact that maximum strain rate of blood flow is in this zone, whereas the minimum is in recirculation zone. In actual fact, vortex core and recirculation in this zone influenced thinning behavior of blood flow which crossed around this zone, while the polymeric part of blood (τ_p in equation (3)) and strain rate of blood affected Newtonian solvent part (τ_s in equation (3)). Comparing all the modes, it was seen that maximum shear rate occurred in the fourth mode near artery wall, but the maximum average of shear rate occurred in the first mode because most fractions of the blood represented a high amount of shear rate. Another important key point in medical investigation of shear stress in arteries is finding injury-prone areas, especially the danger of rapture, which can occur due to high pressure or high shear rates. Therefore, a comparison between the wall shear stress in the four lines considered was done, Fig. 12. Maximum shear rate was seen in Line3 at bifurcation region and in Line 4 after the bulb region. This could be due to maximum velocity and shear rate in these regions. Although in line graphs which plot τ_{xz} and τ_{yz} the measures of the wall shear stress in both Line1 and Line 2 are higher than two other lines, the measures are not significant in comparison with the measures relayed to two other regions in τ_{xx} and τ_{yy}. The results showed that the areas after bulb regions in ECA and ICA, and the bifurcation region between ICA and ECA were areas prone to some arterial diseases, e.g., aneurysm or rapture dangers because of the high shear rate in these areas.

5. Conclusion

The rheology of pulsatile blood flow in carotid artery and shear stress in blood and artery wall were investigated using sPTT viscoelastic model. The whole simulation was done with a finite volume C++ based on open source code, OpenFOAM. It was observed that τ_{xx} and τ_{yy} could have the highest influence on the magnitude of shear stress in the bulb region. The investigation of velocity stream line, velocity profile and shear stress in various sections of carotid artery showed that the maximum shear stress was in the bifurcation region between ECA and ICA and also

after bulb regions in ECA and ICA due to velocity gradients and changes in thinning behavior of blood and increasing strain rate in Newtonian stress part.

References

[1] ADESANYA S.O., MAKINDE O.D., *Irreversibility analysis in a couple stress film flows along an inclined heated plate with adiabatic free surface*, Physica A, 432, 2015, 222–9.

[2] BERNABEU M.O., NASH R.W., GROEN D., CARVER H.B., HETHERINGTON J., KRUGER T., COVENEY P.V., *Impact of blood rheology on wall shear stress in a model of the middle cerebral artery*, Interface Focus, 2013, 3, 20120094.

[3] BOTNAR R.H., RAPPITSCH G., SCHEIDEGGER M.B., LIEPSCH D., PERKTOLD K., BOESIGER P., *Hemo-dynamics in the carotid artery bifurcation: a comparison between numerical simulations and in vitro MRI measurements*, Journal of Biomechanics, 2000, 33, 137–144.

[4] CAMPO-DEANO L., OLIVEIRA M.S.N., PINHO F.T., *A review of computational hemodynam-ics in middle cerebral aneurysms and rheological models for blood flow*, Appl. Mech. Rev., 2015, 67, 1–16.

[5] CHAICHANA T., ZHONGHUA S., JEWKES J., *Computational fluid dynamics analysis of the effect of plaques in the left coronary artery*, Comput. Math. Methods Med., 2012, 504367.

[6] CIBIS M., POTTERS W.V., SELWANESS M., GIJSEN F.J., FRANCO O.H., ARIAS L. ANDRES M., DE BRUIJNE M., HOFMAN A., VAN DER LUGT A., NEDERVEEN A.J., WENTZEL J.J., *Relation between wall shear stress and cardiol artery wall thickening MRI versus CFD*, Journal of Biomechanics, 2016, 49, 5, 735–741.

[7] CAMPO-DEANO C., DULLENS R.P.A., AARTS D.G.A.L., PINHO F.T., OLIVEIRA M.S.N., *Viscoelasticity of blood and viscoelastic blood analogues for use in polydymethylsiloxone in vitro models of the circulatory system*, Biomicrofluidics, 2013, 7, 034102.

[8] FIELDMAN J.S., PHONG D.H., AUBIN Y.S., VINET L., *Rheology, Biology and Mechanics of Blood Flows*, Part II: *Mechanics and Medical Aspects*, Springer, 2007, 115–123.

[9] HAYAT T., IQBAL M., YASMIN H., ALSAADI F., *Hall effects on peristaltic flow of couple stress fluid in an inclined asymmetric channel*, Int. J. Biomath., 2014, 7, 1–34.

[10] JOZWIK K., OBIDOWSKI D., *Numerical simulations of the blood flow through vertebral arteries*, Journal of Biomechanics, 2009, 43, 85–177.

[11] KARIMI S., DABAGH M., VASANA P., DADVAR M., DABIR B., JALALI P., *Effect of rheological models on the hemodynamics within human aorta: CFD study on CT image-based geometry*, Journal of Non-Newtonian Fluid Mechanics, 2014, 207, 42–52.

[12] LARIMI M.M., RAMIAR A., RANJBAR A.A., *Numerical simulation of magnetic nano-particles targeting in a bifurcation vessel*, J. Magn. Magn. Mater, 2014, 362, 58–71.

[13] LARIMI M.M., RAMIAR A., RANJBAR A.A., *Magnetic nanoparticles and blood flow behavior in non-Newtonian pulsating flow within the carotid artery in drug delivery application*, Journal of Engineering in Medicine, 2016, DOI: 10.1177/0954411916656663.

[14] LASSALINE J.V., MOON B.C., *A computational fluid dynamics simulation study of coronary blood flow affected by graft placement*, Inter. Cardiovasc. Thorac. Surg., 2014, 1–5.

[15] LIU X., FAN Y., DENG X., ZHAN F., *Effect of non-Newtonian and pulsatile blood flow on mass transport in the human aorta*, J. Biomech., 2011, 44, 1123–1131.

[16] MAKINDE O.D., *Asymptotic approximations for oscillatory flow in a tube of varying cross section with permeable isothermal wall*, Rom. J. Phys., 2007, 52(1–2), 59–72.

[17] MEKHEIMER K.S., *Peristaltic flow of a couple stress fluid in an annulus: application of an endoscope*, Physica A, 2008, 387, 2403–2415.

[18] MISRA J.C., PANDEY S.K., *Peristaltic transport of blood in small vessels: study of a mathematical model*, Comput. Math. Appl., 2002, 43, 1183–1193.

[19] MORBIDUCCI U., PONZINI R., GALLO D., BIGNARDI C., RIZZO G., *Inflow boundary conditions for image-based computational hemodynamics: impact of idealized versus measured velocity profiles in the human aorta*, J. Biomech., 2013, 46, 102–109.

[20] BURATTI P., *Analysis of Doppler blood flow velocity in carotid arteries for the detection of atherosclerotic plaques*, PhD Thesis Politecnico di Milano, 2011.

[21] PRAKASH O., MAKINDE O.D., SINGH S.P., JAIN N., KUMAR D., *Effects of stenoses on non-Newtonian flow of blood in blood vessels*, Int. J. Biomath., 2015, 8(1), 1550010, DOI: 10.1142/S1793524515500102.

[22] PRAKASH J., MAKINDE O.D., *Radiative heat transfer to blood flow through a stenotic artery in the presence of magnetic field*, Lat. Am. Appl. Res., 2011, 41(3), 273–7.

[23] REDDY J.V.R., SRIKANTH D., MURTHY S.K., *Mathematical modelling of couple stresses on fluid flow in constricted tapered artery in presence of slip velocity-effects of catheter*, Appl. Math. Mech., 2014, 35, 947–58.

[24] SINHA A., MISRA J.C., *MHD flow of blood through a dually stenosed artery: effects of viscosity variation, variable hematocrit and velocity slip*, Can. J. Chem. Eng., 2014, 92, 23–31.

[25] SUD A.K., SEKHON G.S., MISHRA R.K., *Pumping action on blood by a magnetic field*, Bull. Math. Biol., 1977, 39, 385–390.

[26] SRIVASTAVA L.M., SRIVASTAVA V.P., *Peristaltic transport of blood: Casson model II*, J. Biomech., 1984, 17, 821–829.

[27] TORTORA G.J., DERRICKSON B., *The Cardiovascular System: Blood Vessels and Hemodynamics*, [in:] G.J. Tortora, B. Derickson (eds.), *Principles of Anatomy and Physiology*, 13th ed., John Wiley & Sons, 2012, p. 8216.

[28] TORTORA G.J., DERRICKSON B., *The Cardiovascular System: Blood Vessels and Hemodynamics*, Laminar Flow Analysis, John Wiley & Sons, 2012.

[29] WILDE D.D., TRACHET B., MEYER G.D., SEGERS P., *The influence of anesthesia and fluid–structure interaction on simulated shear stress patterns in the carotid bifurcation of mice*, Journal of Biomechanics, 2016, 49, 13, 2741–2747.